ABHATH AL-YARMOUK: "*Basic Sci. & Eng.*" Vol. 16, No.1, 2007, pp. 1-17

Use of X-ray Diffraction and Mud Master Program in the Evaluation of Crystallite Size and Size Distributions of Illite and Kaolinite at Various Depths of Rock Formations in Jordan

Ibrahim M. Odeh*, Waleed A. Saqqa and Denis Eberl*****

Received on March 29, 2006 **Accepted for publication on Nov. 5, 2006**

Abstract

The mean crystallite size (CS_{mean}), mean thickness (T_{mean}) and crystallite thickness distributions (CTD) for illite (I) and kaolinite (K) have been determined for representative Jordanian mudrock samples of different ages. MudMaster analyses of the X-ray diffraction (XRD), based on the Bertaut-Warren-Averbach (BWA) method, have been employed in the calculations. The CS_{mean} and T_{mean} for illite show a slight increase with a mean difference of +0.5nm and +1.4nm respectively with the increase of the present-day stratigraphic thicknesses (depths) of rock formations. An increase in the CS_{mean} and T_{mean} of kaolinite proceeds only to certain depths (1.22km, 1.05km respectively). Beyond these depths, the two means flip with a mean difference of -0.7nm, -2.1nm, respectively, when the depth reaches 1.6km. The shapes of crystallite thickness distributions (CTD) for illite in all investigated mudrock samples are asymptotic. The asymptotic shape more likely mirrors the overlapping reflections of different generations of illite and mixed layer I-S phases. Shapes of CTD for kaolinite vary between asymptotic, multimodal and lognormal. This is more likely due to the presence of two generations of kaolinite growth coinciding with increasing depths of the rock formations.

Keywords: X-ray diffraction, mudrock, kaolinite, illite, MudMaster, BWA-method, crystallite size, asymptotic, multimodal, lognormal.

Introduction

The use of X-ray diffraction (XRD) to study the crystalline structure of clay minerals, crystallite size - and shape of crystallite thickness distributions (CTDs) has attracted considerable attention over the past years. Crystallite size is a measurement of adjacent, repeating crystalline units. It is only equivalent to the grain size if the individual grains are perfect single crystals free of defects, grain boundaries or stacking faults. Crystallite size is determined by measuring the broadening of a particular XRD

* Department of Physics, , Yarmouk University, Irbid, Jordan.

** Department of Earth & Environmental, Faculty of Sciences, Yarmouk University, Irbid, Jordan.

*** U.S. Geological Survey, 3215 Marine St., Boulder, CO 80303-1066 USA.

peak associated with a particular planar reflection from within the crystal unit cell. It is inversely related to the FWHM (full width at half maximum) of the peak. The narrower is the peak, the larger the crystallite size. This is due to the periodicity of the individual crystallite domains, in phase, reinforcing the diffraction of the X-Ray beam, resulting in a tall narrow peak. If the crystal are defect free and periodically arranged, the X-Ray beam is diffracted to the same angle even through multiple layers of the specimen. If the crystallites are randomly arranged or have low degree of periodicity, the result is a broader peak. Crystallite thickness refers to the mode of stacking two or more crystals of a clay mineral. The Bertaut-Warren Averbach (BWA) method is adapted to study clay minerals having a periodic structure along the c-axis. The XRD-peak shapes for the *00l* reflections are then analyzed to calculate the crystallite thickness distributions (CTD_s). The shape of the CTD_s is used to infer crystal growth mechanism undergone by clay minerals during diagenesis or alteration by applying a simulation technique. Dudek et al. [1] pointed to several mathematical approaches in order to obtain information about crystallite size from the XRD peak shapes. The Scherrer equation [2], variance method [3, 4], Voigt method [5] and Bertaut-Warren-Averbach (BWA) method [6, 7] are applied to determine crystallite size using the XRD spectra. The BWA-method is the most universal because it can be used to measure the crystallite size, strain and crystallite size distributions. The MudMaster, a computer program utilizing a version of the BWA-method is applied to carry out such measurements [6, 7]. The evolution of illite as a function of burial diagenesis can be better explained by applying the BWA-method [6, 7, and 8]. The shapes of crystallite thickness distributions (CTD), asymptotic, lognormal and multimodal, may provide information regarding nucleation and crystal growth mechanisms of clay minerals [2, 6, 7, and 8].

The main task of the present study is to determine the mean crystallite size and thickness of illite and kaolinite from the XRD data and to interpret the shapes of size distributions from the *001* basal reflections in the XRD spectra. The MudMaster with the aid of the BWA-method has been extensively utilized for this purpose.

Materials and Methods

Representative mudrock samples were selected from different sites in Jordan as shown in Fig. (1). The samples represent the late Ordovician-early Silurian Batra Member kaolinitic claystone (Batn el-Ghol area), black shale of late Permian Umm Irna Formation (Dead Sea area), the gray-green kaolinitic claystone from the Lower Cretaceous Kurnub Group (Mahis area), the green claystone of the Turonian Shueib Formation (Tafila area), the red-brownish claystone of the Pleistocene and Al-Yamaniyya clay deposits (Al-Yamaniyya, Aqaba area). The abbreviations: SIL, UI, MAH, TAF, and YAM in the text are derived from the original names of the studied rock formations or their ages. They indicate the Silurian Batra Member claystone, Umm Irna black shale, Mahis, Tafila and Al-Yamaniyya clay deposits respectively.

The samples were gently crushed using an agate mortar and pestle. They were then treated with 12% H_2O_2 to remove organic matter. After oxidation, samples were wet sieved using a test sieve of 45μm to separate coarser fractions. The clay fraction (<2 μm) obtained from the pass 45μm fraction by sedimentation, centrifugation and dialysis was

sedimented on a polished silicon substrate and left to dry at room temperature. After mounting on the substrates, air-dried samples were heat treated separately at 350°C and 550°C. Vaporization of ethylene glycol was used to saturate clay samples at 60°C for 16 hours. PVP-10 intercalated air-dried clay samples were analyzed by XRD for the purpose of measuring the fundamental illite particle size and size distribution [9]. The ratios of PVP to clay intercalations were as follows:

Sample	Ratio PVP : CLAY
YAM	4:1
TAF	3:1
MAH	2:1
UI	2:1
SIL	2:1

Clay fraction was suspended in distilled water (concentration 2.5mg clay/1ml H_2O), mixed with an aqueous solution containing 5mg PVP/1ml H_2O and fully dispersed by ultrasonic treatment. The proportion of clay to PVP used depended on the expandability of the clay sample. The larger the proportion of smectite layers the more PVP was added to obtain good intercalation [1]. The advantage of the PVP-10 intercalation was to remove the effect of peak broadening related to swelling interface of the exposed basal surfaces of illite. In this way, crystallite size can be accurately calculated by the BWA-method. The use of silicon substrates improved the background of the XRD spectra [7, 9, and10]. The *001* reflection of PVP-illite and kaolinite were used to measure mean crystallite size (Cs_{mean}), mean crystallite thickness (T_{mean}) and crystallite thickness distributions [6, 8, and 11]. XRD diffraction spectra were carried out using a Phillips PW1710 Diffractometer equipped with copper tube, CuKα radiation, and a theta compensatory slit assembly. The diffractometer was operated under the following experimental conditions: a voltage of 35 KV, beam current of 40mA , step size of 0.02 2θ, counting time of 0.01sec/step, 1mm receiving slit and a scanning range of 2-65° 2θ. The BWA-method adapted in the MudMaster computer program is based on Fourier analysis of the interference function [2, 6].

Lithology of mudrocks

Fig (2) illustrates the graphic logs for the different rock formations. The Batra Member of Late Ordovician-early Silurian (Batn el-Ghol, SE Jordan) consists of light gray-green kaolinitic clays with Graptolite remains along bedding planes. Reddish siltstone-fine sandstone beds intercalate the green clays with a total thickness of about 80m. The occurrence of Graptolite indicates marine origin [12]. The Umm Irna Formation of late Permian (Dead Sea area) consists principally of two quartz arenite sandstone facies (60 m. thick) with fining upward cycles. Each starts with pebbly sandstone at the base, changes upward into fine sandstone, siltstone and silty claystone. The uppermost two cycles are distinguished by the presence of reddish-brown and occasionally dark gray paleosol horizons separated from each other by dark gray-black

shale beds with plant remains [13]. The Lower Cretaceous Kurnub Group (Mahis area) consists of a thick varicolored sandstone sequence (≈200m.) interbedded with kaolinitic clay beds. The Turonian Shueib Formation (Karak-Tafila area) consisting of green and red gypsiferous claystone beds interbedded with gypsum changes near the top to fossiliferous dolomitic limestone. The Al-Yamaniyya Pleistocene clay deposits consist of varicolored (gray, green, yellow, red-brown) claystone interbedded with pebbly-coarse-fine sandstone beds. Al-Yamaniya clay deposits were more likely deposited in a nearshore environment [Note 1, 14, 15].

Experimental results

a. XRD analysis

The XRD diffraction patterns (Fig.3; Table 1) show that smectite (S) dominates other clay minerals in YAM claystone samples. The other clay minerals are kaolinite (K), illite (I), mixed layer illite-smectite (I-S), chlorite (Ch) and mixed layer illite-chlorite (I-Ch). The *001* peak of S at 6.2° 2θ (14.25A°) in air-dried samples expands to 5° 2θ (17.67A°) after ethylene glycol saturation. The same peak collapsed upon heating at 550°C to 9.04° 2θ (9.8A°). Peaks of Ch and mixed layer I-Ch are apparent in heated samples as shown in Figure (3).

In TAF clays, a broad peak appears in air-dried mounts at 8.02° 2θ (11.02A°). This is more likely to be a mixture of 'I' and one-water layer S. After glycolation, the peak shifts to 5.4° 2θ (16.37A°) and a new *001* peak of illite appears at 8.8° 2θ (10A°). When heating at 550°C, the broad peak at 11.02A° collapsed to 10A°. Kaolinite is also present in the TAF green claystone.

In the UI black shale and MAH clay samples, asymmetric broad and low intensity mixed-layer I-S peaks appear at 7.7° 2θ (11.5A°) and 7.2° 2θ (12.3A°) together with I and K. The mixed layer I-S peaks collapsed upon heating (550°C) to 8.8° 2θ (10A°). Illite and kaolinite are dominant in the SIL clays.

b. Crystallite size of illite and kaolinite versus depth

Table (2) summarizes the results of mean crystallite size (CS_{mean}), mean thickness (T_{mean}) and CTD shapes of illite and kaolinite. The CS_{mean} (2.8nm-3.3nm) and T_{mean} (3.8nm-5.2nm) for illite show a slight increase (+0.5nm, +1.4nm respectively) with increasing depth of the rock formations (Fig.4.a). The CS_{mean} and T_{mean} for kaolinite are somewhat different. The means of the two values range between 3nm-10.7nm and 7.5nm-16.8nm, respectively. A slight increase in the CS_{mean} of K (+ 0.7 nm) occurs when the depth changes from shallow to 0.95km. This is followed by an abrupt increase from 3.7nm-9.0nm (+5.3nm) when depth is 1.05km.

The CS_{mean} increases by 1.7nm when the depth changes from 1.05km to1.22km. Beyond the 1.22km depth, the mean size flips (- 0.7 nm.) when the depth is 1.6km (Fig.4.b). The T_{mean} for kaolinite increases from 7.5nm to 11.3nm (+3.8nm) going from a shallow depth to 0.95km. The T_{mean} abruptly increases to 16.8nm (+5.5nm) at a depth of 1.05km and then eventually decreases to 14.7nm (-2.1nm) beyond this depth (Fig. 4.b).

c. Crystallite thickness distributions (CTD) for illite and kaolinite

The crystallite thickness distributions (CTD) for air-dried PVP-illite and heated (350°C) kaolinite samples were determined using MudMaster analysis based on the BWA- method ,area-weighted option [9]. Figures (5 and 6) illustrate the shapes of CTD for PVP-I and K respectively. The CTD shapes in PVP-I was asymptotic in all samples. This is more likely a result of overlapping reflections of different generations of illite and I-S phases in clay deposits [16]. Another view point relates the asymptotic shape to the great influence of simultaneous nucleation and crystal growth of illite [17, 18]. This is only very likely, if illite in the samples represents one generation devoted to one mechanism of formation [18]. However, the later explanation needs more investigation. The CTD shapes of kaolinite vary from asymptotic (YAM and TAF clays) to multimodal (MAH clays) and lognormal (UI and SIL clays). This variation reflects the occurrence of two generations for kaolinite growth in response to changes in depth from shallow to deep. Otherwise, the variation in the CTD can be explained on how the crystal growth mechanism of kaolinite alters from a constant rate nucleation accompanied with crystal growth (at shallow-moderate depths) to crystal growth without continuous nucleation (at greater depths) [17, 18].

Discussion

Results of X-ray analyses give an initial impression on how the type and abundance of clay minerals in the investigated mudrock samples vary with the present-day stratigraphic thicknesses of rock formations (depths). Mineralogically, smectite predominates other clay minerals in Al-Yamaniyya Pleistocene superficial clay deposits, but deficient in the Tafila green claystone of the Turonian Shueib formation and the Lower Cretaceous Mahis clay deposits occurring at depths around one km. Smectite more likely changed to mixed layer I-S in the Tafila claystone. In the Lower Cretaceous Mahis clays, kaolinite predominates other clay minerals and illite is less dominant. Progressive illitization is possibly enhanced at depths over 1 km. Therefore, strong peaks of illite and kaolinte were typical in the late Permian Umm Irna black shale (depth of rock formation approximates 1.2km) and in the Upper Ordovician-Lower Silurian green claystone of Batra Member (depth around 1.6km). The distinct appearance of illite peaks in the Paleozoic mudrocks indicates diagenetic alterations of smectite and mixed layer S-I precursors to illite. The degradation of smectite and its transformation to illite involve incorporation of potassium (K^+) ions into smectite structure and loss of interlayer water [19, 20]. The compaction of mud through overburden pressure soon removes much of the water contained in clay mineral lattices and water adsorbed onto clay surface or the less common pore-filled water. At depths greater than one kilometer (temperature ≥45°C), 70-90% of the original volume of water is reduced to about 30%. Further compaction through water loss requires temperature of about 100°C (depths 2-4km) where dehydration of clays takes place causing some changes in clay mineral types [21, 22}. Final compaction, leading to mudrock formation with only small percent water needs much longer period of overburden pressure with elevated temperatures [22]. Despite the significant role of temperature and burial history in clay diagenesis, the role of tectonic uplift and sediment unroofing cannot be ignored. Another criterion which

may complicate the origin of clay minerals is the possible occurrence of the same types of clay minerals in more than one particular environment (terrestrial-marine). This is despite differences in the physical and chemical conditions.

In this work, we consider the issue of primary (detrital) origin of clay minerals of paramount importance. For instance, the coexistence of kaolinite and smectite in Al-Yamaniyya clay deposits can be explained on the basis of their primary origin after chemical weathering of source materials. The latter minerals are very likely weathering products of the very near Precambrian granites intruded by mafic dikes. Products of weathering were then transported by streams draining granite terrains and finally deposited in a lacustrine environment separated from sea by beach terraces [14, 15, and 23]. Leaching of iron and magnesium in source area leaves behind concentrations of silicon and aluminum. This is favorable for kaolinite formation.

In the Tafila mudrocks, the presence of dolomite and gypsum beside the argillaceous sediments signifies a deposition in a coastal sabkha environment after an uplift at the beginning of the Turonian age. The tectonic event caused sea-level fall resulting in the development of the sabkha environment [24]. The Tafila mudrocks were more likely deposited during periodic influxes of fresh water which may facilitate illitization process [e.g. 25]. The green type of Tafila clays were possibly developed by leaching of nearby red clays and reduction of hematite under surface conditions. This idea can be supported by the absence of chlorite (not detected by X-ray analyses) from the green clays which can also impart green color for clay deposits in nature. We do believe that Tafila clays were subjected to illitization as a result of surface wet-dry cycles, evaporation, and fixation of K^+ ions. The lack of sodium chloride (NaCl) in the depositional medium (absence of halite in the rock sequence) enhances K^+ ions fixation in clays [26]. A burial depth of about one kilometer may help the transformation of smectite to mixed layer I-S. Many researchers [e.g. 27, 28, 29, 30] believe that illitization of smectite through I-S can take place under surface conditions when lake water becomes alkaline and saturated with K^+ ions whereby wet-dry cycles and evaporation eventually lead to irreversible fixation of K^+ ions and illite formation.

Mahis kaolinitic clay deposits that are a part of fluvial system sediments [31], have two origins, detrital (primary) and authigenic. Khouri [23] mentioned neoformation of kaolinite flakes adhered to quartz grains surfaces in Mahis clay sediments. Intensive leaching of the detritus in acidic medium helps kaolinization aided by rainfall water. Field observations confirmed a presence of carbonized plant remains in Mahis clays. The breakdown of plant remains due to compaction releases CO2 and creates acidic pore water. This initiates neoformation of kaolinite at depths greater than 1km (T>50°C). The minor content of I-S and the initial presence of illite in Mahis clays suggest advanced stages of illitization at such depths. Coalified plant remains are also found in the Late Permian Umm Irna black shale. This again prompts the creation of acidic medium in the pore-filling water as a result of organic matter decay and CO2 release possibly by thermal maturation at greater depths (>1200m). Accordingly, crystal growth of a primary kaolinite can take place. The strong appearance of illite and kaolinite peaks present in the XRD patterns supports the idea of precursor smectite illitization and the increase of kaolinite crystallinity with depth. The great compaction of green claystone and

sandstones of the Upper Ordovician-Lower Silurian Batra Member by overlying rocks (present-day depth>1.6km) undoubtedly produced a set of physical and chemical changes on these sediments. Hence, illitization process is continued and the crystallinity of K is well developed.

Summary and conclusions

The present work revealed that diagenetic changes of clay minerals in the investigated mudrock samples took place at various depths. The occurrence of smectite gradually diminished with depth and was replaced by illite through an intermediate stage of mixed-layer I-S. Transformations between clay minerals could be produced under different depositional settings regardless of the evolved physical and chemical conditions. For instance, the illitization of Tafila clays in a saline environment was enhanced by wet-dry cycles, evaporation, and K^+-ions fixation at surface conditions. Burial depths and the increase of subaerial temperature were essential for illite crystallization and the increase of kaolinite crystallinity. The asymptotic CTD shape in illite indicates, at most, an overlap between different generations of illite and mixed layer I-S in clays. The variations in CTD shape of kaolinite (asymptotic, multimodal, and lognormal) explain the occurrence of two generations of kaolinite growth coincident with the continual increase of the present-day depths of the rock formations.

Acknowledgments

The authors would like to thank Dr. F. Ababneh from Physics Department, Yarmouk University for helping, partly, in operating the X-ray Diffractometer. We extend our appreciation to the anonymous referees for their comments and critique in advance.

استخدام مطيافية حيود الأشعة السينية والبرنامج المحوسب (MudMaster) في إيجاد الحجم البلوري وتوزيع الأحجام البلورية للايلايت والكاولينايت على اعماق مختلفة للتكاوين الصخرية في الأردن.

ابراهيم محمد عودة، وليد عبد القادر السقا ودينس د. ابريل

ملخص

فقد تم استخدام مطيافية حيود الأشعة السينية والبرنامج المحوسب "مد ماستر" لتحديد متوسط الحجم البلوري ومتوسط السماكة البلورية، وأنماط توزيع السماكات البلورية لحبيبات الإيلليت

والكاؤلينيت في عينات تمثل صخور طينية مختلفة الأعمار من الأردن. أظهرت الدراسة زيادة طفيفة في متوسط الحجم البلوري ومتوسط السماكات البلورية لحبيبات الإيلليت تتناسب مع تزايد أعماق التكاوين الصخرية الحالية. أما بالنسبة لحبيبات الكاؤلينيت، فتستمر الزيادة في متوسط الحجم البلوري ومتوسط السماكات البلورية إلى أعماق تصل إلى 1.22كم، 1.05كم على التوالي. يتناقص كل من متوسط الحجم والسماكات البلورية عندما يصل العمق 1.6كم. يأخذ منحنى التوزيع الإحصائي لسماكة بلورات الإيلليت قي جميع العينات النمط المحاذي مما يشير إلى تداخلات مختلفة من أجيال الإيلليت ومختلط الطبقات إيليت-سميكتيت. أما بالنسبة لشكل منحنى توزيع السماكات البلورية لحبيبات الكاؤلينيت، يتفاوت بين النمط المحاذي، ومتعدد النماذج، واللوغارتمي الطبيعي، الأمر الذي يعزى إلى تنوع أطوار نمو بلورات الكاولينيت مما يتوافق مع زيادة أعماق التكوينات الصخرية.

References

[1] Dudek T., Środoń J., Eberl D.D., Elsass F. and Uhlik P., Thickness distribution of illite crystals in shales. Part 1: X-ray diffraction *vs*. high-resolution transmission electron microscopy measurements. *Clays and Clay Minerals,* 50 (2002) 562-577.

[2] Drits V.A., Środoń J., and Eberl D.D., XRD measurement of mean crystallite thickness of illite and illite/smectite; reappraisal of the Kubler index and the Scherrer equation. *Clays and Clay Minerals,* 45 (1997) 461-475.

[3] Wilson A. J.C., *Proc. Phys. Soc*. 80 (1962) 286; ibid. 81 (1963) 41.

[4] Árkai P., Merriman R.J., Roberts B., Peacor D.R. and Tóth M., Crystallinity, crystallite size and lattice strain of illite-muscovite and chlorite: comparison of XRD and TEM data for diagenetic to epizonal pelites. *European Journal of Mineralogy,* 8 (1996)1119-1138.

[5] Langford J. I., *J. Appl. Cryst.* 11 (1978). 10-14.

[6] Eberl D.D., Drits V.A., Środoń J. and Nüsch R., MudMaster: a program for calculating crystallite size distribuition and strain from the shapes of X-ray diffraction peaks. *U.S. Geological Survey*, *Open-File Report,* (1996) 96-171.

[7] Drits V.A., Eberl D.D. and Środoń J., XRD measurement of mean thickness, thickness distribution and strain for illite and illite/smectite crystallites by the Bertaut-Warren-Averbach technique. *Clays and Clay Minerals,* 46 (1998) 38-50.

[8] Brime C., Eberl D.D. and Środoń J., Growth mechanisms of low-grade illites based on the shapes of crystal thickness distributions. *Schwarz. Mineral. Petrogr. Mitt.,* 82 (2002) 203-209.

[9] Eberl D.D., Nüsch R. Šucha, V. and Tsipursky S., Measurement of illite particle thicknesses by X-ray diffraction using PVP-10 intercalation. *Clays and Clay Minerals,* 46 (1998b) 89-97.

[10] Bove D.J., Eberl D.D., McCarty D.K. and Meeker G.P., Characterization and modeling of illite crystal particles and growth mechanism in a zoned hydrothermal deposit, Lake City, Colorado. *American Mineralogist,* 87 (2002) 1546-1556.

[11] Šucha V., Kraus I., Šamajová E. and Puskelova L. Crystallite size distribution of kaolin minerals. *Periodico di Mineralogia,* 68 (1999) 81-92.

[12] Abed A., *Geology, Environment and water of Jordan (in Arabic).* Jordanian Geological Association, Scientific Books Series 1, Amman, (2000) 571.

[13] Makhlouf I., Turner B. and Abed A.M., Depositional facies and environments in the Permian Umm Irna Formation, Dead Sea area, Jordan. *Sedimentary Geology,* 73 (1991) 117-139.

[14] Abu Halima K., Mineralogy, chemistry and industrial studies of Al-Yamaniyya clay deposits in Aqaba area. Unpublished M.Sc. thesis, University of Jordan, Amman (1993).

[15] Saqqa W.A., Dwairi I.M. and Akhal H. M. Sedimentology, mineralogical evaluation and industrial applications of the Pleistocene Al-Yamaniyyah clay deposits, near 'Aqaba, southern Jordan. *Applied Clay Science* 9, (1995) 443-458.

[16] Środoń J., Precise identification of illite/smectite interstratifications by X-ray powder diffraction. *Clays and Clay Minerals,* 28 (1980) 401-411.

[17] Eberl D.D., Drits V.A. and Środoń J. Deducing growth mechanisms for minerals from the shapes of crystal size distributions. *American Journal of Science*, 298(1998a) 499-533.

[18] Środoń J., Eberl D.D. and Drits V.A. Evolution of fundamental-particle size during illitization of smectite and implications for reaction mechanism. *Clays and Clay Minerals,* 48 (2000) 446-458.

[19] Dunoyer de Segonzac, G. The transformation of clay minerals during diagenesis and low grade metamorphism: a review. *Sedimentology*, 15, (1970)281-346.

[20] Hower J., Elsinger E.V., Hower M.E. and Perry E.A., Mechanism of burial metamorphism of argillaceous sediment: 1. Mineralogical and chemical evidence. *Bulletin of Geological Society of America,* 87(1976) 725-737.

[21] Tucker M., *Sedimentary Petrology: An introduction*. Blackwell Scientific Publications, Oxford, (1981) 252pp.

[22] Tucker M., *Sedimentary Petrology: an introduction to the origin of sedimentary rocks*. 2nd edition, Blackwell Scientific Publications LTD, Oxford, (1991). 260pp

[23] Khouri H.N., *Clays and Clay Minerals in Jordan*. Published by University of Jordan, Amman, (2002)116.

[24] Abed A. and El-Hiyari M., Depositional Environments and Paleogeography of the Cretaceous gypsum horizon in west-central Jordan. *Sedimentary Geology,* 47(1986)109-123.

[25] Droste J.B. Clay mineral composition of evaportie sequences. *Northen Ohio Geological Society,* 1(1963)47-54.

[26] Honty M., Uhlik P., Šucha V., Čaplovičová M., Franců J., Clauer N. and Biroň A., Smectite-to-illite alteration in salt-bearing bentonites (The east Slovak basin). *Clays and Clay Minerals,* 52(2004)533-551.

[27] Stoffers P. and Singer A., Clay minerals in Lake Mobuto Seso Seko (Lake Albert) – their diagenetic changes as an indicator of the paleoclimate. *Geologische Rundschau,* 68(1979)1009-1024.

[28] Eberl D.D., Środoń J. and Northrop H.R., Potassium fixation in smectite by wetting and drying. In: *Geochemical Processes at Mineral Surfaces* (J.A. Davis and K.F. Hayes, editors). ACS Symposium Series 323, American Chemical Society, (1986) 296-326.

[29] Hay R.L. and Guldman S.G., Silicate diagenesis in sediments of Searles Lake, California. *Clay Mineral Society Progress with Abstracts*, *Jackson*, MS 15, (1986).

[30] Turner C.E. and Fishman N.S., Jurassic Lake T'oo'dichi': a large alkaline saline lake, Morrison Formation, eastern Colorado Plateau. *Geological Society of America Bulletin*, 103 (1991) 538-558.

[31] Abed A., Depositional environments of the Early Cretaceous Kurnub (Hathira) Sandstones, North Jordan. *Sedimentary Geology*, 31, (1982) 267-271.

Note 1: Ibrahim K. And Abdelhamid G., Al-Yamaniyya clay deposits. Unpublished Report, *Natural Resources Authority*, Amman, 1990.

Table (1) : Summary for XRD data between 3°-15 ° 2θ.

Name of Sample	Air-dried (2θ)	Air-dried (*dA°*)	(*dA°*)	Ethylene-glycolated (2θ)	Ethylene-glycolated (*dA°*)	(*dA°*)	Heated (550°C) (2θ)	Heated (550°C) (*dA°*)	Clay mineral
YAM	6.2	14.25	shifted to	5.0	17.67	collapsed to→	9.04	9.8	S
	n.d.	n.d.	→	n.d.	n.d.	→	6.54	13.5	I-Ch.
	8.88	10	slightly increased to	8.68	10.10	slightly shifted to	9.04	9.8	I
	n.d.	n.d.	→	10.3	8.6	shifted to	9.04	9.8	I-S
	12.42	7.13	→	12.2	7.25	→	12.62	7.02	Ch
	12.48	7.09	→	12.34	7.17	→	destroyed		K
TAF	8.02	11.02	separated to two peaks:	1) 5.2 2) 8.8	17.0 10.0	1)collapsed to 2) unchanged	8.8 8.8	10.0 10.0	Mixture of I and one layer S. S
	12.32	7.18	unchanged	12.32	7.18	→	destroyed		I K
MAH	6.92	12.7	separated to two peaks:	1) 5.4 2) 7.2	16.3 12.3	1)collapsed to 2) →	8.8 →	10.0	I-S S I-S
	8.8	0.0	slightly shifted to	9.04	9.78	unchanged	8.8	10	I
	12.38	7.15	unchanged	12.38	7.15	→	destroyed		K
UI	7.7	11.5	unchanged	7.7	11.5	collapsed to	8.8	10	I-S
	8.94	9.89	unchanged	8.94	9.89	unchanged	8.94	9.89	I
	12.4	7.13	unchanged	12.4	7.13	→	destroyed		K
SIL	8.92	9.91	v. little change	9.02	9.8	unchanged	8.92	9.91	I
	12.44	7.12	unchanged	12.48	7.2	→	destroyed		K

(n.d. = non detected, S = smectite, I = illite, I-S = mixed layer illite-smectite, Ch = chlorite, I-Ch= mixed layer illite-chlorite, K= kaolinite).

Table (2): D-spacing of the *001* reflection, means of crystallite size (CS_{mean}) and thickness (T_{mean}) and CTDs shapes of PVP-illite and kaolinite *vs*. depths.

(A) PVP-illite (air-dried samples)

Sample	Depth(m)	Mean size(nm)	Thickness(nm)	d-spacing(A□.	CTDs
			(nm)	(A□.	shape
YAM	shallow	2.8	3.8	10.07	Asymptotic.
TAF	950	3	4	9.83	Asymptotic
MAH	1050	2.9	4	10.12	Asymptotic
U I	1220	3	4.1	10.03	Asymptotic.
SIL	1600	3.3	5.2	10.09	Asymptotic

(B) Kaolinite (heated samples at 350°C)

Sample	Depth (m)	Mean size (nm)	Thickness(nm)	d-spacing(A□	CTDs shape
YAM	shallow	3	7.5	7.13	Asymptotic
TAF	950	3.7	11.3	7.17	Asymptotic
MAH	1050	8.9	16.8	7.17	Multimodal
U I	1220	10.7	14.7	7.13	Lognormal
SIL	1600	10	14.7	7.16	Lognormal

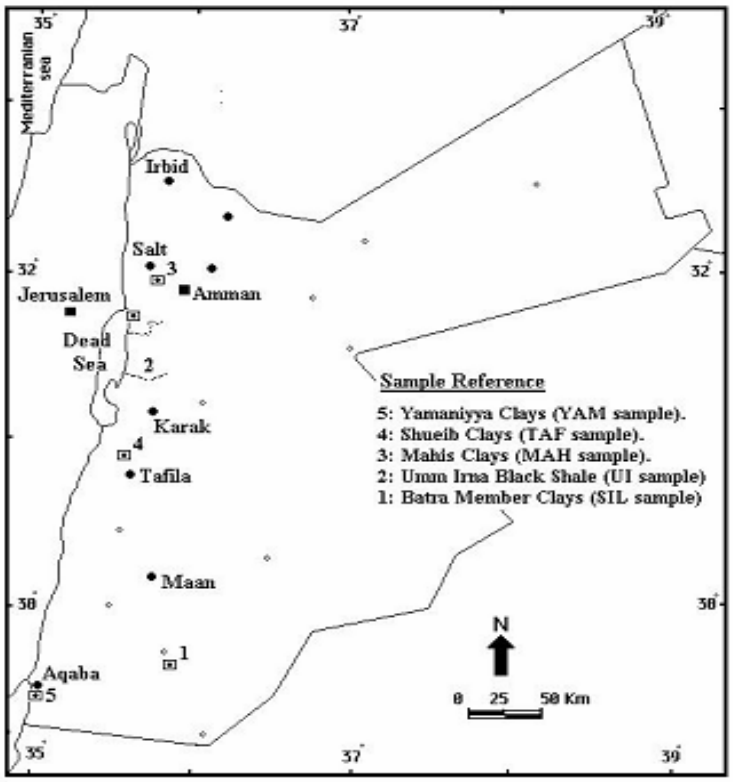

Fig. (1) Locations of study samples.

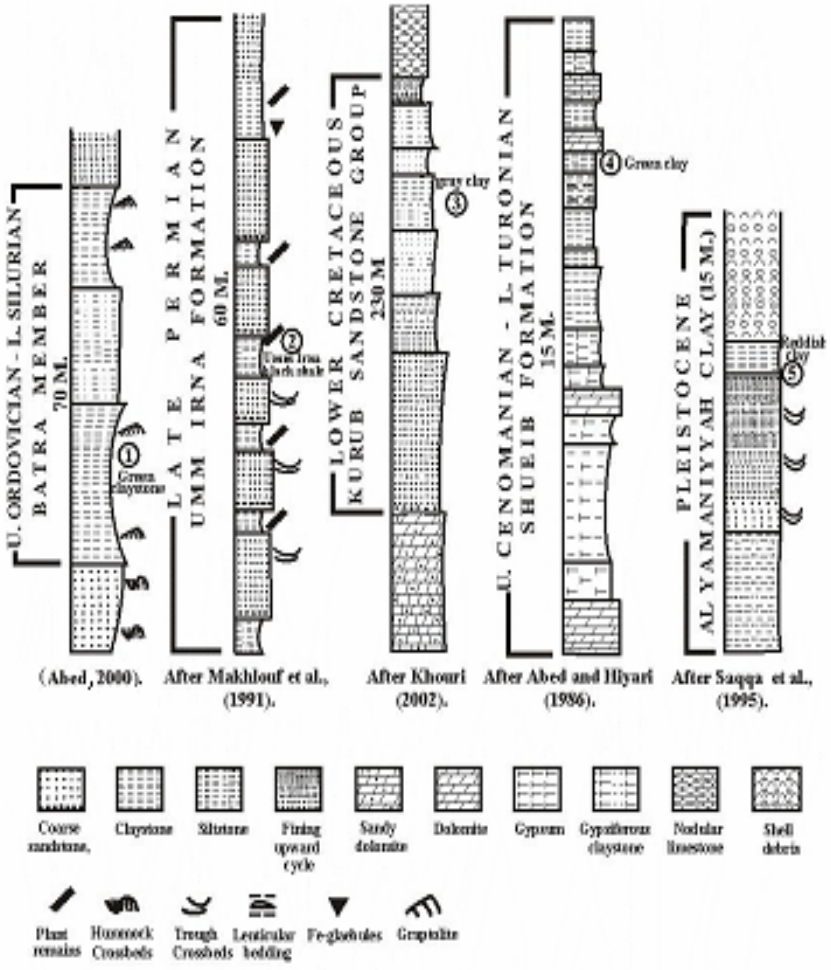

Fig. 2. Generalized columnar sections from which mudrock samples were selected. {(Reference samples denoted in text as: SIL (sample 1), UI (sample 2), MAH (sample 3), TAF (sample 4), YAM (sample 5)}.

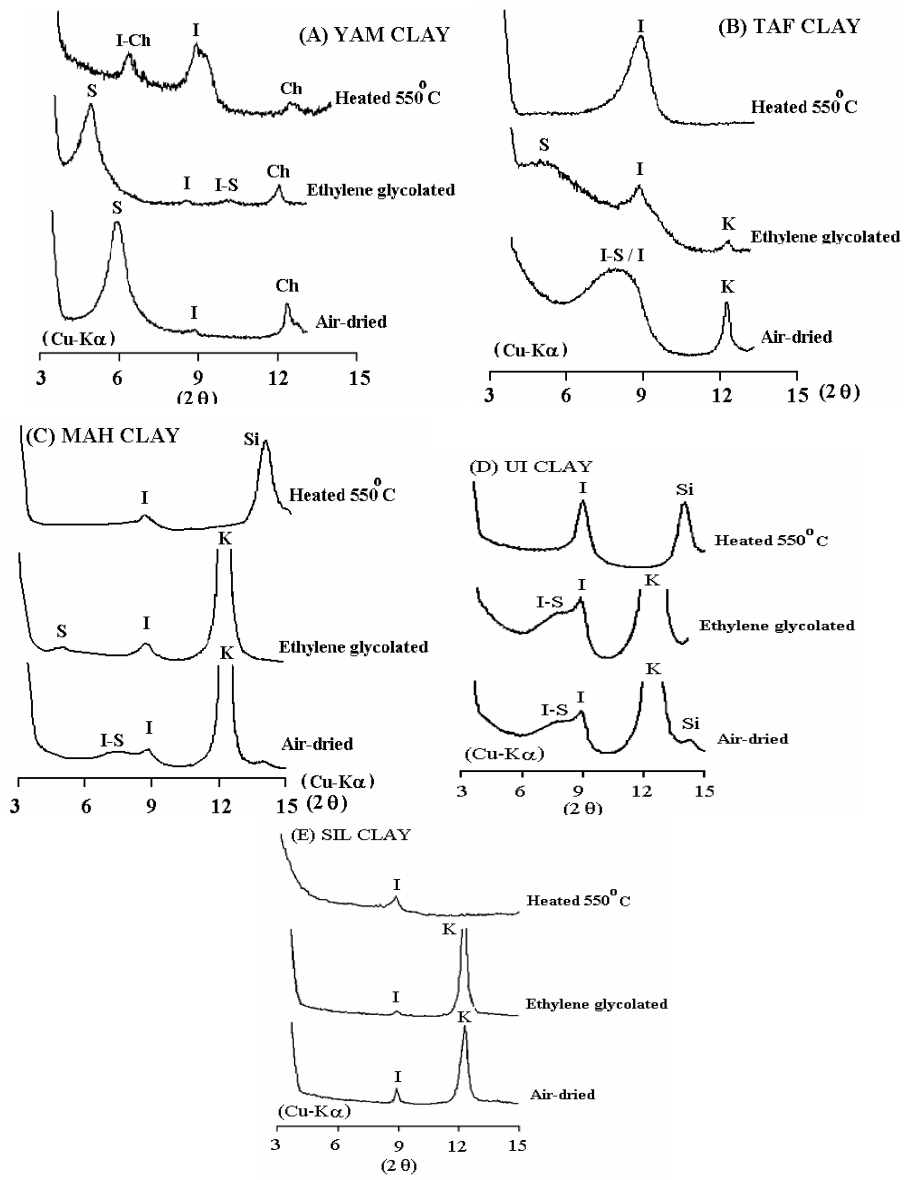

Fig.3. XRD-patterns (air-dried, ethylene glycolated, heated at 550°C) of study samples. S=smectite, I-S= mixed layer illite-smectite, I=illite, K=kaolinite, Ch =chlorite, I-Ch= mixed layer illite-chlorite, Si = silicon wafer

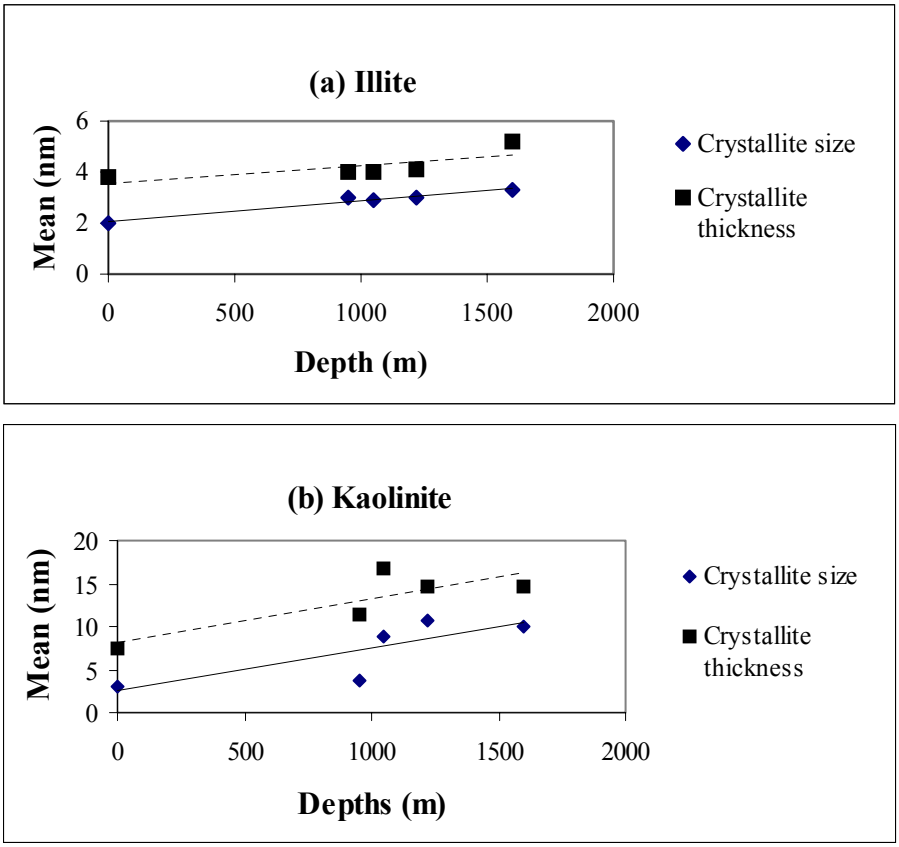

Fig.4. Means of crystallite size and thickness for illite (a) and kaolinite (b) vs. depths.

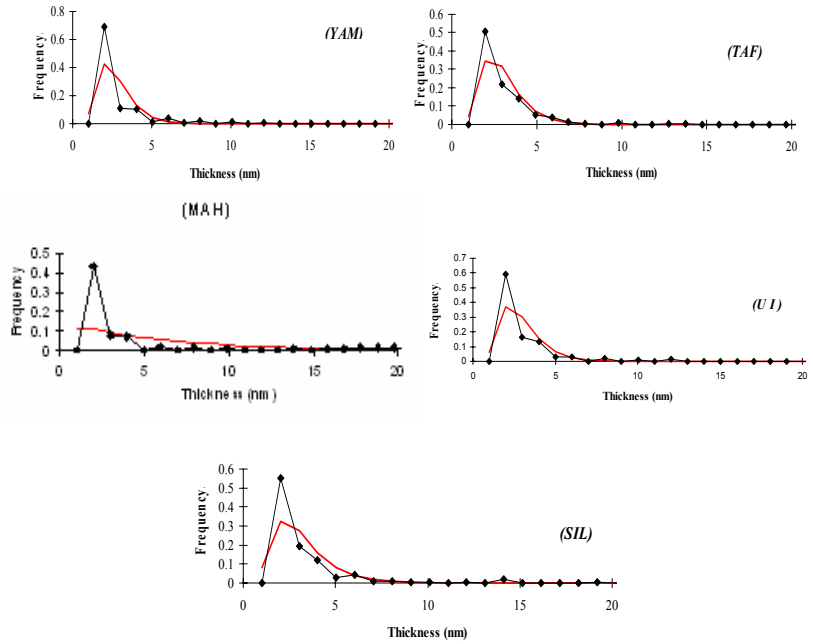

Fig. 5. Shapes of PVP-Illite crystallite thickness distributions (CTDs) in the study samples using the BWA-method (MudMaster).

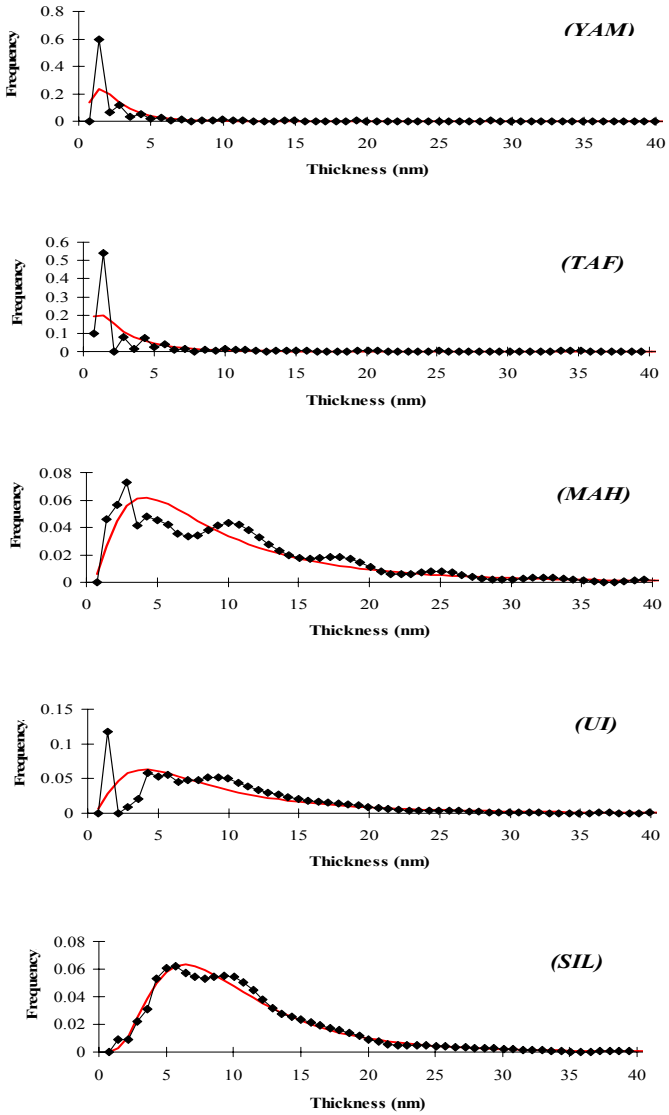

Fig. 6. Shapes of kaolinite crystallite thickness distributions (CTDs) in the study samples using BWA-method (MudMaster).